

Supporting Information for

Enhanced Menshutkin S_N2 Reactivity in Mesoporous Silica: The Influence of Surface Catalysis and Confinement

Weizhong Zheng^{†,‡,1}, Steven A. Yamada^{†,1}, Samantha T. Hung[†], Weizhen Sun[‡], Ling Zhao^{**‡}, and Michael D. Fayer^{*†}

[†]Department of Chemistry
Stanford University, Stanford, CA 94305, USA
*Phone: (650) 723-4446; Email: fayer@stanford.edu

[‡]State Key Laboratory of Chemical Engineering
East China University of Science and Technology, Shanghai 200237, China
**Phone: (021) 64253175; Email: zhaoling@ecust.edu.cn

¹W.Z. and S.A.Y. contributed equally to this work.

SI. Experimental Methods and Analysis

A. Surface Areas, Pore Size Distributions, and Pore Volumes

The investigated mesoporous silica samples include MCM41 with 2.8 nm pores (ACS Material), SBA15 with 4.2 nm (Sigma Aldrich) and 8.3 nm pores (ACS Material), and the passivated MCM41 (MCM41-Si(Me)₃) with 2.3 nm pores. The MCM41, MCM41-Si(Me)₃, and SBA15 samples were characterized by their N₂ (g) sorption isotherms taken at the Soft & Hybrid Materials Facility (SMF) at the Stanford Nano Shared Facilities (SNSF). The N₂ (g) sorption isotherms and pore diameter distributions are displayed in Figs. S1a and S1b, respectively, for the 8.3 nm SBA15 and 2.3 nm MCM41-Si(Me)₃. The relevant plots for the other pore sizes are part of a future publication. The surface areas of these materials were calculated from the adsorption curves using the BET method.^{1,2} BJH analysis on the sorption isotherms was used to obtain the pore diameters, which are narrowly distributed (Fig. S1b). Analysis of the adsorption or desorption curves gave identical results. The surface areas, pore sizes, and total pore volumes are listed in Table 1. The MCM41-Si(Me)₃ displays a smaller pore size, surface area, and pore volume relative to the as received MCM41 owing to the replacement of surface OH groups with larger -Si(Me)₃ groups. This is supported by the FT IR spectrum of the passivated material, which exhibits CH₃ symmetric (2904.3 cm⁻¹) and antisymmetric (2962.5 cm⁻¹) stretching modes (Fig. S2). Residual absorbance due to the silanol hydroxyl stretch in the ~3450-3500 cm⁻¹ region was still observed following the passivation reaction, indicating that the passivation was

incomplete.

B. Synthesis of MCM41-Si(Me)₃

To elucidate the effect of the silanol groups on the confined Menshutkin reaction, the pore surface of MCM41 was passivated. The hydroxyl groups on the pore wall of MCM41 (2.8 nm) were modified with trimethylsilyl chloride (ClSi(Me)₃), according to previous procedures.³⁻⁵ 0.2 g of dry MCM41 powder was dispersed in 10 mL of toluene, followed by the addition of ClSi(Me)₃ in 5-fold excess. The resultant mixture was stirred at ca. 110 °C under refluxing conditions for 30 h. The modified MCM41 was filtered and washed with toluene several times to remove the excess ClSi(Me)₃ and then was dried at ~200 °C under vacuum (~100 mTorr) for 24 h. The MCM41-Si(Me)₃ product was analyzed using FT IR spectroscopy (Figure S2). The antisymmetric CH₃ stretch mode is found at 2962.5 cm⁻¹, in agreement with that reported previously (2962 cm⁻¹).⁶ Another lower frequency mode is observed at 2904.3 cm⁻¹, which we assign to the symmetric CH₃ stretch mode.⁷

C. Sample Preparation and TGA Analysis

For the bulk sample, MeSCN and MeIm were mixed in a scintillation vial at a molar ratio of 1:10 in a glovebox and stirred for 5 min. To prepare the powdered sample, the bulk solution was gently mixed with completely dry MCM41 (or SBA15) for 30 min in the glovebox. The particles were vacuum filtered for 1 min under a N₂ (g) atmosphere. The filtered sample was equilibrated in a home-built flow chamber (Fig. S3), which was successfully used to hydrate the MCM41 pores with water in a previous publication.² Nitrogen gas was bubbled through 1:10 MeSCN:MeIm solution and flowed over the powder. The vapor pressure of the reactants was sufficient to condense inside of the pores but low enough to remove the bulk liquid on the exterior of the particles. The equilibration time was kept as short as possible (~3-4 h) to ensure the reaction did not progress significantly. Samples prepared in this way exhibited reproducible percent mass losses as verified through Thermogravimetric Analysis (TGA). These data are plotted for the different size pores in Fig. S4. The mass loss of the dry materials were in the range 3-5 %. Taking this into account, and using the measured mass losses and pore volumes, the solution densities inside of the pores were calculated to be 1.00 ± 0.07, 1.1 ± 0.1, 0.99 ± 0.07 and 1.2 ± 0.1 g/mL for the regular 2.8, 4.2, 8.3 nm materials and passivated 2.3 nm MCM41-

Si(Me)₃ system, respectively. The estimated densities are comparable to those of pure MeIm and MeSCN, with values of 1.032 and 1.074 g/mL, respectively.

D. Sample Cell Assembly and Linear IR Spectroscopy

The sample cell assembly for the linear IR experiments was detailed in a previous paper.² The bulk reaction mixture was sandwiched between two 3 mm thick, 25.4 mm diameter CaF₂ windows separated by one 12 μm polytetrafluoroethylene (PTFE) ring spacer of the same diameter. For the powdered samples, two concentric PTFE spacers with outer diameters of 25.4 and 13 mm were used. The powder was placed in the region enclosed by the inner spacer. Paraffin oil was employed as an index matching fluid to cover the sample and fill the region between the inner and outer spacers, which isolated the sample from water. Linear absorption spectra were measured using FT IR spectroscopy with a Thermo Scientific Nicolet 6700 FT IR spectrometer, which is purged with CO₂ and H₂O free air. To study the reaction kinetics, the spectra were acquired every 30 min for the initial 20 h of the reaction. The sample was then heated up to 356.2 K and the spectra were taken until the reaction was complete.

E. Rate Constant Determination

The reaction of methyl thiocyanate (MeSCN) with 1-methylimidazole (MeIm) to form the ionic liquid 1,3-dimethylimidazolium thiocyanate (MmimSCN)



is an S_N2 reaction involving the alkylation of a nitrogen, or Menshutkin reaction (Fig. 1a).⁸ The nitrogen lone pair of the MeIm nucleophile attacks the methyl group of MeSCN, resulting in the loss of the SCN⁻ leaving group and formation of the Mmim⁺ cation. The rate-limiting step depends on the concentrations of MeIm and MeSCN, making the reaction rate second order overall^{8,9}

$$\text{rate} = k_1[\text{MeIm}][\text{MeSCN}], \quad (\text{S2})$$

where k_1 is the forward rate constant with units M⁻¹s⁻¹.

In this work, MeIm serves as both reactant and solvent. In the pure solvent, [MeIm] = 12.5 M. In a 1:10 MeSCN:MeIm mixture, assuming the density is equal to that of the pure solvent, [MeSCN] = 1.25 M. Therefore, [MeIm] remains approximately constant over the

course of the reaction, particularly at early time, and Eq. (S2) can be approximated as a pseudo-first order reaction¹⁰

$$\text{rate} = k[\text{MeSCN}], \quad (\text{S3})$$

where $k = k_1[\text{MeIm}]$. Rewritten in terms of $[\text{SCN}^-]$, Eq. (S3) reads

$$\text{rate} = \frac{d[\text{SCN}^-]}{dt} = k([\text{MeSCN}]_i - [\text{SCN}^-]), \quad (\text{S4})$$

where $[\text{MeSCN}]_i$ is the initial MeSCN concentration. The solution to Eq. (S4) is

$$[\text{SCN}^-] = [\text{MeSCN}]_i(1 - e^{-kt}). \quad (\text{S5})$$

Thus, the rate constant k can be determined by monitoring the formation of the SCN^- product as a function of time. The CN stretch vibration of SCN^- can be easily monitored through FT IR spectroscopy. The CN stretch band area, A_{SCN^-} , is related to $[\text{SCN}^-]$ through Beer's law

$$A_{\text{SCN}^-}(t) = \ell \int \varepsilon(\omega)c(\omega,t)d\omega$$

$$[\text{SCN}^-] = \int c(\omega,t)d\omega, \quad (\text{S6})$$

where ℓ is the sample path-length, and $\varepsilon(\omega)$ and $c(\omega,t)$ are the frequency-dependent extinction coefficient and SCN^- concentration, respectively. When the reaction is complete, $[\text{SCN}^-]_f = [\text{MeSCN}]_i$. Therefore,

$$[\text{SCN}^-] = [\text{MeSCN}]_i \frac{A_{\text{SCN}^-}(t)}{A_{\text{SCN}^-}(t \rightarrow \infty)}. \quad (\text{S7})$$

To simplify the determination of the rate constant, k , we analyze the short time behavior of Eq. (S5). When combined with Eq. (S7), this gives the fractional yield of SCN^- as

$$\frac{[\text{SCN}^-]}{[\text{MeSCN}]_i} = \frac{[\text{SCN}^-]}{[\text{SCN}^-]_f} = \frac{A_{\text{SCN}^-}(t)}{A_{\text{SCN}^-}(t \rightarrow \infty)} \approx kt. \quad (\text{S8})$$

F. Transition State Theory

The temperature-dependent rate constant for a thermally activated process can be described by the Arrhenius equation

$$k = Ae^{-E_a/RT}, \quad (\text{S9})$$

where A , E_a , and R are the pre-exponential factor, activation energy, and ideal-gas constant, respectively.

Eyring's transition-state theory (TST) expression for the rate constant at fixed pressure^{11,12} is given by,

$$k_{TST} = \frac{k_B T}{hc^\circ} K^\ddagger = \frac{k_B T}{hc^\circ} e^{-\Delta^\ddagger G^\circ/RT}, \quad (\text{S10})$$

where k_B , h , c° , K^\ddagger , and $\Delta^\ddagger G^\circ$ are respectively the Boltzmann constant, Planck's constant, the standard-state concentration (usually 1.00 M), the equilibrium constant between the transition state and reactants, and the standard free energy of activation. The inclusion of c° accounts for the bimolecular nature of the Menshutkin reaction considered here and ensures the correct dimensions.¹³ In general, this factor is $c^{\circ(m-1)}$, where m is the number of reacting molecules. The derivation of k_{TST} assumes that the reactants and transition-state are in equilibrium, and that there is zero re-crossing of the dividing surface once products are formed.¹² As seen in Eq. (S10), the higher the concentration of the activated complex relative to that of the reactants (i.e. the larger the value of K^\ddagger), the larger the rate constant. For a bimolecular ideal-gas phase reaction, Eq. (S10) can be written in a form analogous to Eq. (S9),¹³

$$k_{TST} = \frac{e^2 k_B T}{hc^\circ} e^{\Delta^\ddagger S^\circ/R} e^{-E_a/RT}, \quad (\text{S11})$$

where $\Delta^\ddagger S^\circ$ is the standard entropy of activation. Comparison of Eqs. (S9) and (S11) shows that the prefactor A is related to $\Delta^\ddagger S^\circ$, where positive and negative values of $\Delta^\ddagger S^\circ$ indicate that the transition state is respectively more or less "disordered" relative to the reactants.

It is important to note that the conventional TST expression cannot account for non-idealities such as high pressure and solvent effects,¹⁴ which are clearly important to the Menshutkin reaction.^{8,9,15,16} Kramers later extended the theory by modeling a chemical reaction as a classical particle of mass, m , moving in a one dimensional asymmetric double-well potential $U(x)$.^{12,17} The position of the particle, x , represents the reaction coordinate. Kramers incorporated the remaining degrees of freedom of the surrounding molecules as a heat bath at temperature T , which influences the reaction coordinate through a fluctuating force $\xi(t)$ (Brownian motion) and a damping force $-m\gamma\dot{x}$, where γ represents a constant damping rate (friction). For moderate-to-strong friction, he obtained the following result for the rate constant,

$$k = \kappa k_{TST} = \frac{(\gamma^2/4 + \omega_b^2)^{1/2} - \gamma/2}{\omega_b} k_{TST}, \quad (\text{S12})$$

where ω_b^2 is related to the curvature of the potential at the position of the transition state.^{12,17} The term κ is called the transmission coefficient. κ accounts for re-crossing of the barrier from products to reactants, which lowers the rate constant. In Kramer's theory, multiple random re-crossings can occur, while in TST the barrier is crossed only once during the reaction coordinate's motion to the product side. In the regime of moderate-to-strong friction, as γ becomes small, κ approaches unity, and Eyring's original expression k_{TST} is obtained. For nonzero γ , κ is always less than unity, showing that k_{TST} is an upper bound on the rate constant.

Combining the results of Eyring and Kramers, the prefactor A can be expressed as

$$A = \left[\frac{(\gamma^2/4 + \omega_b^2)^{1/2} - \gamma/2}{\omega_b} \right] \frac{e^2 k_B T}{hc} e^{\Delta^\ddagger S^\circ/R}. \quad (\text{S13})$$

III. Simulation Details

A. Classical MD Simulations

The silica pore models were constructed by cutting a cylindrical nanopore out of a block of amorphous silica. The dangling-bond O and Si on the surface of the pores were saturated with H and OH groups, following the same strategy as previous reports.¹⁸⁻²⁰ The density of silanol groups was 4.8 ± 0.3 sites/nm², which is in good accord with the measured value (4.9 ± 0.5 sites/nm²) for silica surfaces.²¹ The pore diameters are 2.8, 4.2, and 8.3 nm, with cell dimensions of $4.28 \times 4.28 \times 4.28$, $6.42 \times 6.42 \times 4.28$, and $11.2 \times 11.2 \times 4.28$ nm³, respectively. Bulk MeIm boxes of the same x and y dimensions as the corresponding pore models were built using the Packmol program.²² The silica pore models were filled by placing them between two bulk MeIm boxes. The resultant box was equilibrated under the canonical (NVT) ensemble with a Berendsen thermostat at 296.2 K for 40 ns. It was found that the pores were fully filled with MeIm after 20 ns. Liquid molecules outside of the pores were removed if their z -coordinates were less than those of the outermost silica atoms in the $+$ and $-z$ directions. One MeIm molecule in the center

of the pore was replaced by the MeSCN molecule, resulting in 180, 430, and 1620 MeIm molecules, respectively, for the 2.8, 4.2, and 8.3 nm pores, as shown in Fig. 1b. Although the MeSCN concentration in the simulations is lower than in the experiments, we found that the FT IR line shape and rotational and spectral diffusion dynamics of the MeSCN solute measured with polarization selective pump-probe and 2D IR spectroscopy on very dilute solutions were identical to the same quantities in the 1:10 MeSCN:MeIm solutions. The combined box was further equilibrated under the *NVT* ensemble with the temperature maintained at 296.2 K using a Nose-Hoover thermostat with a time constant of 200 fs. Three 40 ns trajectories were run with a time step of 1 fs. The last 20 ns were used to extract the properties of interest.

The interactions between the silica pore, confined MeIm, and MeSCN solute were represented by Lennard-Jones (L-J) and Coulombic interactions. The L-J parameters were taken from the ClayFF model to represent the pore systems,²³ and from the OPLS-AA force field for MeIm and MeSCN. The L-J potential for the C and N atoms of the SCN group of MeSCN were replaced by the ANL model.²⁴ The structures of MeIm and MeSCN were optimized at the B3LYP/6-311G(d,p) level, and the ChelpG charges were refit from the optimized geometries at the same level using the Gaussian 09 program.²⁵ Instead of the original charges from the ClayFF model, the smaller charges from the LR model were used for the pore,¹⁸ which gave better agreement with the measured reorientational anisotropy of MeSCN measured in the PSPF experiments. The force field parameters for the silica pore models are provided in Table S2. All the classical simulations were performed using GROMACS.²⁶ Lorentz-Berthelot mixing rules were employed with periodic boundary conditions (PBC) in three dimensions. During the simulations, the silica frame was held fixed, while the angles and dihedral angles of the Si-OH and Si(OH)₂ groups on the pore surface were made flexible using parameters detailed previously.² The Si-O and O-H bond lengths of the Si-OH and Si(OH)₂ groups were fixed at 1.54 and 0.98 Å. The particle mesh Ewald method with a cut-off radius of 1.2 nm was used to treat the long-range electrostatic interactions for all the systems. The initial velocities were randomly generated from a Maxwell-Boltzmann distribution and the LINCS algorithm was utilized to constrain the covalent bonds including hydrogen atoms.

B. Reaction Energy Profile Calculations

To elucidate the influence of surface silanols on the reaction of MeIm with MeSCN, DFT

calculations were performed to analyze the reaction energy profile in the hypothetical gas phase system and on the silica surface system without solvent. An optimized model silica surface from a previous study, referred to as SiO₂-3 with 4.6 OH per nm²,²⁷ was used to represent the silica pore surface and obtain reliable results at minimum computational cost. The unit cell of the 001 surface model is 21.39×21.39×13.70 Å³. To eliminate interactions between surface images in the *z* dimension, a vacuum slab ca. 26 Å thick was added in the *z*-direction, giving a final unit cell 21.39×21.39×40 Å³ in size, as shown in Fig. 9a. For the gas phase system, the CR and CP binding complexes were optimized and subsequently the transition states (TS) were calculated via the Dimer method.²⁸ The adsorption of MeSCN onto the hydroxylated silica surface is a key step initiating the surface reaction. Therefore, the MeSCN position and orientation on the surface were optimized and the most stable configuration was determined. MeIm was then added at the proper position close to the methyl group of MeSCN to calculate the surface CR. An analogous strategy was employed to calculate the surface CP. The TS calculation was conducted following the same method used for the gas phase system.

The electronic structure calculations were simulated using CP2K. The Gaussian and plane waves (GPW) method with Goedecker-Teter-Hutter pseudopotentials²⁹ was adopted and the DZVP-MOLOPT-GTH basis set was employed for all the atoms with an energy cutoff of 350 Ry.²⁷ The exchange-correlation functional complemented by Grimme D3 dispersion corrections was treated by the GGA-PBE method, and the convergence thresholds for the total energy and SCF calculations were maintained at 10⁻¹⁰ and 10⁻⁸ hartree, respectively.³⁰ For the structure optimization and transition state calculations, the convergence criteria for the gradient and displacement were set to 5×10⁻⁵ hartree/bohr and 1×10⁻⁴ bohr, respectively.

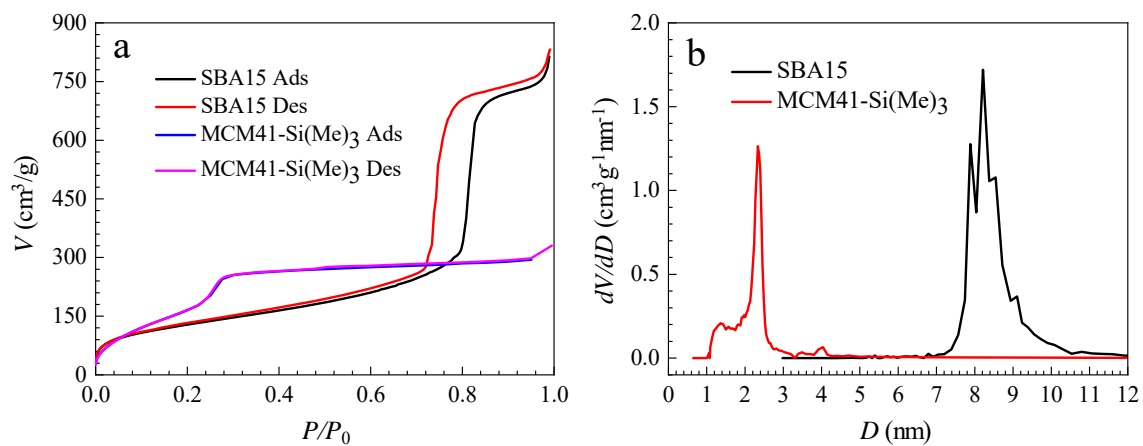


Figure S1. (a) N_2 (g) adsorption and desorption isotherms. (b) Pore diameter distributions obtained from BJH analysis³¹ of the curves in (a).

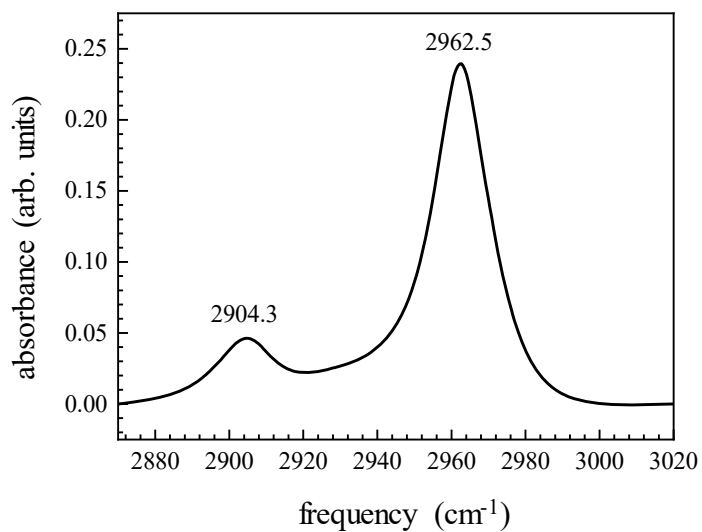


Figure S2. Background subtracted linear-IR spectrum of MCM41-Si(Me)₃.

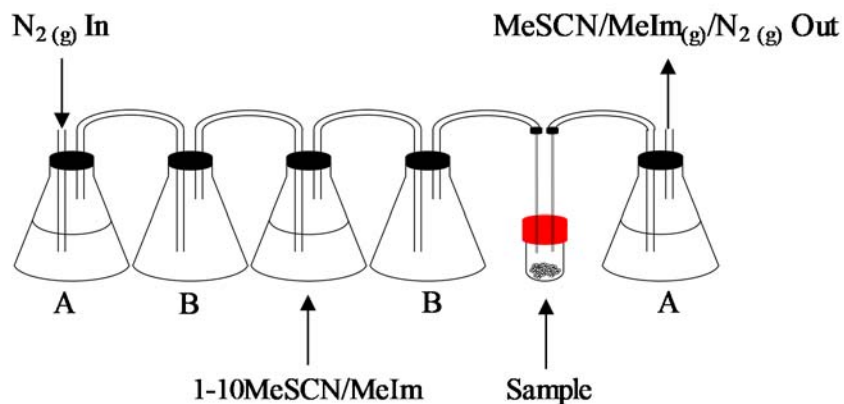


Figure S3. Home-built flow chamber used to condense the MeSCN/MeIm reaction mixture inside MCM41 and SBA15 mesoporous silica: A = Mineral Oil, B = empty. For clarity, only one flask containing 1:10 MeSCN:MeIm solution is depicted, whereas two were typically used in series to ensure complete equilibration of the solution vapor pressure in the N_2 stream.

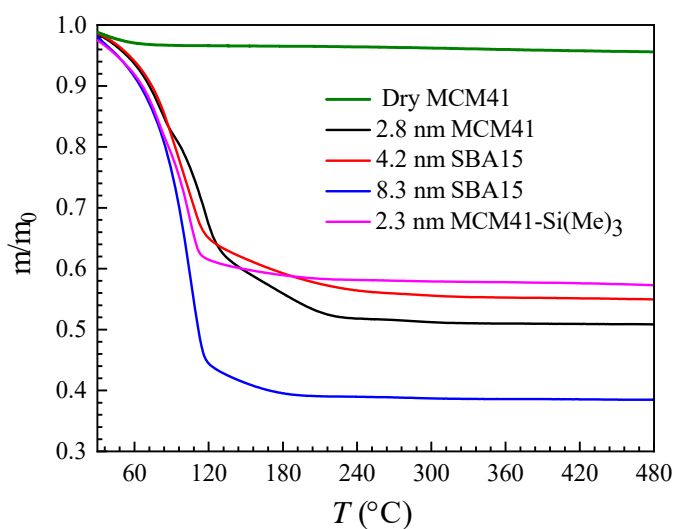


Figure S4. TGA traces for dry MCM41 and 1:10 MeSCN:MeIm solution confined in silica pores of different sizes.

Table S1. Reactant complex (CR), transition state (TS), and product complex (CP) distance parameters (nm) in the gas phase and pore systems.

bonds	bulk phase			pore surface		
	CR	TS	CP	CR	TS	CP
N2-C1	0.320	0.190	0.147	0.299	0.200	0.147
C1-S1	0.183	0.254	0.358	0.182	0.242	0.342
N1-H2	-	-	0.163	-	-	0.209
S1-H (Silanol)				0.240	0.232	0.216
N1-H (Silanol)				0.185	0.177	0.178
N1-H (Silanol)				0.198	0.187	0.198

Table S2. Silica Pore Force Field Parameters

atom	(Å)	(kJ/mol)	(e)
Si	0.33020	0.0000077	1.24
^a O _b	0.31656	0.65000	-0.620
O	0.31656	0.65000	-0.710
H	0.12950	0.00155	0.400
angle	<i>k</i> (kJ/mol/rad ²)		(deg)
Si-O-H	104.2314		118.5
HO-Si-OH	159.7196		118.5

^aO_b indicates a bridging, or siloxane, oxygen

References

- (1) Brunauer, S.; Emmett, P. H.; Teller, E. Adsorption of gases in multimolecular layers. *J. Am. Chem. Soc.* **1938**, *60*, 309.
- (2) Yamada, S. A.; Shin, J. Y.; Thompson, W. H.; Fayer, M. D. Water Dynamics in Nanoporous Silica: Ultrafast Vibrational Spectroscopy and Molecular Dynamics Simulations. *J. Phys. Chem. C* **2019**, *123*, 5790.
- (3) Jaroniec, C. P.; Kruk, M.; Jaroniec, M.; Sayari, A. Tailoring Surface and Structural Properties of MCM-41 Silicas by Bonding Organosilanes. *J. Phys. Chem. B* **1998**, *102*, 5503.
- (4) Anwender, R.; Nagl, I.; Widenmeyer, M.; Engelhardt, G.; Groeger, O.; Palm, C.; Röser, T. Surface Characterization and Functionalization of MCM-41 Silicas via Silazane Silylation. *J. Phys. Chem. B* **2000**, *104*, 3532.
- (5) Antochshuk, V.; Jaroniec, M. Adsorption, Thermogravimetric, and NMR Studies of FSM-16 Material Functionalized with Alkylmonochlorosilanes. *J. Phys. Chem. B* **1999**, *103*, 6252.
- (6) Yasmin, T.; Müller, K. Synthesis and surface modification of mesoporous mcm-41 silica materials. *J. Chromatogr. A* **2010**, *1217*, 3362.
- (7) Bui, T. X.; Kang, S.-Y.; Lee, S.-H.; Choi, H. Organically functionalized mesoporous SBA-15 as sorbents for removal of selected pharmaceuticals from water. *J. Hazard. Mater.* **2011**, *193*, 156.
- (8) Abboud, J. L. M.; Notario, R.; Bertran, J.; Sola, M. In *Progress in Physical Organic Chemistry*; Taft, R. W., Ed.; John Wiley & Sons: New York, 1993; Vol. 19, p 1.
- (9) Auriel, M.; de Hoffmann, E. Quantitative study of solvent effects on the Menshutkin reaction between 1,4-diazabicyclo[2.2.2]octane and 2-chloroethylbenzene, 2-bromoethylbenzene, and 2-iodoethylbenzene. Part 2. Mixed solvents. *J. Chem. Soc., Perkin Trans. 2* **1979**, 325.
- (10) Knight, A. W.; Tigges, A. B.; Ilgen, A. G. Adsorption of copper (II) on mesoporous silica: the effect of nano-scale confinement. *Geochem. Trans.* **2018**, *19*, 13.
- (11) Eyring, H. The Activated Complex in Chemical Reactions. *J. Chem. Phys.* **1935**, *3*, 107.
- (12) Hänggi, P.; Talkner, P.; Borkovec, M. Reaction-rate theory: fifty years after Kramers. *Rev. Mod. Phys.* **1990**, *62*, 251.
- (13) McQuarrie, D. A.; Simon, J. D. *Physical Chemistry: A Molecular Approach*; University Science Books: Sausalito, 1997.
- (14) Turner, C. H.; Brennan, J. K.; Johnson, J. K.; Gubbins, K. E. Effect of confinement by porous materials on chemical reaction kinetics. *J. Chem. Phys.* **2002**, *116*, 2138.

- (15) Sola, M.; Lledos, A.; Duran, M.; Bertran, J.; Abboud, J. L. M. Analysis of solvent effects on the Menshutkin reaction. *J. Am. Chem. Soc.* **1991**, *113*, 2873.
- (16) Maran, U.; Pakkanen, T. A.; Karelson, M. Semiempirical study of the solvent effect on the Menshutkin reaction. *J. Chem. Soc., Perkin Trans. 2* **1994**, 2445.
- (17) Kramers, H. A. Brownian motion in a field of force and the diffusion model of chemical reactions. *Physica* **1940**, *7*, 284.
- (18) Bourg, I. C.; Steefel, C. I. Molecular dynamics simulations of water structure and diffusion in silica nanopores. *J. Phys. Chem. C* **2012**, *116*, 11556.
- (19) Pajzderska, A.; Gonzalez, M. A.; Mielcarek, J.; Wąsicki, J. Water Behavior in MCM-41 As a Function of Pore Filling and Temperature Studied by NMR and Molecular Dynamics Simulations. *J. Phys. Chem. C* **2014**, *118*, 23701.
- (20) Kumar, K.; Kumar, A. Enhanced CO₂ Adsorption and Separation in Ionic-Liquid-Impregnated Mesoporous Silica MCM-41: A Molecular Simulation Study. *J. Phys. Chem. C* **2018**, *122*, 8216.
- (21) Zhuravlev, L. The surface chemistry of amorphous silica. Zhuravlev model. *Colloids Surf., A* **2000**, *173*, 1.
- (22) Martínez, L.; Andrade, R.; Birgin, E. G.; Martínez, J. M. PACKMOL: a package for building initial configurations for molecular dynamics simulations. *J. Comput. Chem.* **2009**, *30*, 2157.
- (23) Cygan, R. T.; Liang, J.-J.; Kalinichev, A. G. Molecular models of hydroxide, oxyhydroxide, and clay phases and the development of a general force field. *J. Phys. Chem. B* **2004**, *108*, 1255.
- (24) Gee, P. J.; van Gunsteren, W. F. Acetonitrile revisited: a molecular dynamics study of the liquid phase. *Mol. Phys.* **2006**, *104*, 477.
- (25) Frisch, M. J.; Trucks, G.; Schlegel, H.; Scuseria, G.; Robb, M.; Cheeseman, J.; Scalmani, G.; Barone, V.; Mennucci, B.; Petersson, G. Gaussian 09, Revision D. 01, Gaussian. Inc.: Wallingford, CT **2009**.
- (26) Abraham, M. J.; Murtola, T.; Schulz, R.; Páll, S.; Smith, J. C.; Hess, B.; Lindahl, E. GROMACS: High performance molecular simulations through multi-level parallelism from laptops to supercomputers. *SoftwareX* **2015**, *1*, 19.
- (27) Comas-Vives, A. Amorphous SiO₂ surface models: energetics of the dehydroxylation process, strain, ab initio atomistic thermodynamics and IR spectroscopic signatures. *Phys. Chem. Chem. Phys.* **2016**, *18*, 7475.
- (28) Henkelman, G.; Jónsson, H. A dimer method for finding saddle points on high dimensional

potential surfaces using only first derivatives. *J. Chem. Phys.* **1999**, *111*, 7010.

(29) Allolio, C.; Klameth, F.; Vogel, M.; Sebastiani, D. Ab initio H₂O in realistic hydrophilic confinement. *ChemPhysChem* **2014**, *15*, 3955.

(30) Caratelli, C.; Hajek, J.; Rogge, S. M.; Vandenbrande, S.; Meijer, E. J.; Waroquier, M.; Van Speybroeck, V. Influence of a Confined Methanol Solvent on the Reactivity of Active Sites in UiO - 66. *ChemPhysChem* **2018**, *19*, 420.

(31) Barrett, E. P.; Joyner, L. G.; Halenda, P. P. The Determination of Pore Volume and Area Distributions in Porous Substances. I. Computations from Nitrogen Isotherms. *J. Am. Chem. Soc.* **1951**, *73*, 373.